2019

THE STUDY OF SCANDATE CATHODE AND ITS CHARACTERIZATION UNDER VARIOUS STAGES OF PROCESSING

Xiaomeng Zhang
University of Kentucky, jzhang1222@gmail.com
Digital Object Identifier: https://doi.org/10.13023/etd.2019.024

STUDENT AGREEMENT:

I represent that my thesis or dissertation and abstract are my original work. Proper attribution has been given to all outside sources. I understand that I am solely responsible for obtaining any needed copyright permissions. I have obtained needed written permission statement(s) from the owner(s) of each third-party copyrighted matter to be included in my work, allowing electronic distribution (if such use is not permitted by the fair use doctrine) which will be submitted to UKnowledge as Additional File.

I hereby grant to The University of Kentucky and its agents the irrevocable, non-exclusive, and royalty-free license to archive and make accessible my work in whole or in part in all forms of media, now or hereafter known. I agree that the document mentioned above may be made available immediately for worldwide access unless an embargo applies.

I retain all other ownership rights to the copyright of my work. I also retain the right to use in future works (such as articles or books) all or part of my work. I understand that I am free to register the copyright to my work.

REVIEW, APPROVAL AND ACCEPTANCE

The document mentioned above has been reviewed and accepted by the student's advisor, on behalf of the advisory committee, and by the Director of Graduate Studies (DGS), on behalf of the program; we verify that this is the final, approved version of the student's thesis including all changes required by the advisory committee. The undersigned agree to abide by the statements above.

Xiaomeng Zhang, Student

Dr. John Balk, Major Professor

Dr. Matthew Beck, Director of Graduate Studies

THE STUDY OF SCANDATE CATHODE AND ITS CHARACTERIZATION UNDER VARIOUS STAGES OF PROCESSING

THESIS

A thesis submitted in partial fulfillment of the
requirements for the degree of Master of Science in
Materials Science and Engineering in the College of Engineering
at the University of Kentucky

By

Xiaomeng Zhang

Lexington, Kentucky

Director: Dr. John Balk, Professor of Chemical and Materials Science Engineering

Lexington, Kentucky

December 2018

ABSTRACT OF THESIS

THE STUDY OF SCANDATE CATHODE AND ITS CHARACTERIZATION UNDER VARIOUS STAGES OF PROCESSING

Scandate cathode under various processing stages: scandia nano-powder, tungsten scandia mix powder, sintered and impregnated pellets, were characterized with techniques that included electron microscopy, EDS, XPS, and work function measurements. The size and shape uniformity of nano-scale scandia particles changed from round to square and polyhedron during heat treatment. Reduction in size and improvement in size uniformity as heat treating temperature increased were observed. When determining the highest Sc coverage, three assessment methods were used and with their combined results, it was concluded that set VII had the highest Sc at%. In the sintered pellets, it was observed with SEM that more initial scandia coverage in the mix powder sets corresponded to a larger number of scandia particles distributed over the tungsten surface. The structure of the cross section made on pellet surface was porous which was expected in any functional cathode. Kelvin probe measurements revealed that work function values of sintered pellets were similar and decreased by approximately 0.6 eV after the impregnation. A cross section on the impregnated pellet surface revealed that the pores that existed in sintered pellets were gone and filled with impregnated materials that emerged to the surface during impregnation.

KEYWORDS: Scandate cathode, scandia coverage, characterization under different processing stages, microstructure, chemical analysis, work function.

Xiaomeng Zhang

11/07/2018

Date

THE STUDY OF SCANDATE CATHODE AND ITS CHARACTERIZATION UNDER VARIOUS STAGES OF PROCESSING

By
Xiaomeng Zhang

Dr. John Balk
Director of Thesis

Dr. Matthew Beck
Director of Graduate Studies

11/07/2018
Date

DEDICATION

A special feeling of gratitude to my loving parents, Jiguang and Zhixia who offer unconditional love and support during my graduate study.

ACKNOWLEDGMENTS

I would like to thank my major advisor, Dr. John Balk for his valuable guidance and constant support. I am grateful to my committee members, Dr. Matthew Beck, and Dr. Dusan Sekulic for their excellent advises on my research.

In addition to the technical and instrumental assistance above, I received equally important assistance from my colleagues and friends. My colleagues, Xiaotao Liu, Nicolas Briot, Azin Akbari, Dali Qian, Artashes Ter-Isahakyan, and Tyler Maxwell, provided on-going support throughout the thesis study, as well as technical assistance critical for completing the project in a timely manner. Special thanks to Xiaotao Liu for his expertise and guidance on cathode background review, characterization techniques and analysis. Finally, I wish to thank the industrial sponsors, Andrew Hunt and Claudia Goggin from nGimat LLC, and Daniel Busbaher from 3M Ceradyne for their cooperation and make this project possible.

This work was financially supported via a Phase II STTR award “Reliable Manufacturing of Scandia-Doped Tungsten Powders for Thermionic Cathodes” (ID numbers N00253-17-C-0014), sponsored by the US Navy.

TABLE OF CONTENTS

LIST OF TABLES

LIST OF FIGURES

CHAPTER 1. INTRODUCTION

1.1 Thermionic cathodes and their basic working mechanism

The thermionic cathode serves as the source of electrons in many electronic devices such as vacuum tubes, fluorenone lamps, electron guns in electron microscopes, etc. It emits electrons by heating with a filament and is widely used than that of a cold cathode because of its ability to emit more electrons from the same surface area when heated, while a cold cathode only relies on field emission or secondary electron emission from positive ion bombardment. Thermionic cathodes can be categorized into two types in general: directly heated and indirectly heated. As the name suggests, a directly heated cathodes is heated to emit electrons. The filament is the cathode itself which is made of a thin wire of tungsten or other metals with high melting temperature such as tantalum and rhenium, as shown in Table 1 [1]. Directly heated cathodes are used in high power transmitting vacuum environment. In an indirectly heated cathode, the filament heats a separate cathode consisting of thin metal sheet. Most indirectly heated cathodes are nickel tubes coated with metal oxides and used in low power vacuum environment. In this thesis, scandate cathode, a relatively new-developed directly heated cathodes are studied. The goal is to correlate scandia coverage on surface of tungsten particles in tungsten-scandia pre-sintered powder form and work function enhancement by characterization of the cathode under different processing stages: scandia nano-powder, tungsten-scandia pre-sintered powder, sintered pellets, and impregnated cathode.

Table 1.1 [1] Melting Temperatures, Richardson Constants, and Emission for Different Metals

Metal	T_m (K)	T_m (K) at 10^{-7} torr	Temperature Coefficient ($A/cm^2/T^2$)	ϕ_0 (eV)	Usable Emission (A/cm^2)
W	**3640**	**2520**	80	4.54	$\mathbf{4 \times 10^{-1}}$
Ta	**3270**	**2370**	60	4.10	$\mathbf{6 \times 10^{-1}}$
Re	**3440**	**2330**	700	4.7	$\mathbf{2.6 \times 10^{-1}}$
Mo	2890	1970	55	4.15	5×10^{-3}
C	4400	2030	48	4.35	2×10^{-3}
Pt	2050	1650	170	5.40	2×10^{-8}
Ni	1730	1270	60	4.10	5×10^{-9}
Ba	1120	580	60	2.11	1×10^{-11}

At the surface of a cathode there exists a potential energy barrier that prevents electrons from escaping. When heated, thermionic cathodes can provide electrons with enough energy to escape, causing electron emission. The energy of an electron in a pure metal follows Fermi-Dirac distribution and at 0 Kelvin, energies of all electrons are below Fermi energy. The energy above Fermi level is called the work function. When the pure metal is heated, Fermi-Dirac distribution curve shifts accordingly. As a result, some electrons have energies above Fermi energy and are able to escape from the metal surface into the vacuum environment. This process is the thermionic emission.

The relationship between electron emission and work function are obtained by integrating the Fermi-Dirac distribution at a certain temperature. The integral gives the number of electrons with momentum that is sufficient to escape the metal surface. Richardson-Dushman came up with an equation that describes the emission current density of the escaped electrons:

$$I_0 = 120\, T^2\, e^{\left(-\frac{11600\phi}{kT}\right)}$$

where I_0 is emission current density, a measurement of electron emission, T is temperature in Kelvin, ϕ is the work function, and k is Boltzmann constant. In Richard-Dushman's equation, the change of I_0 is dominated by the exponential term rather than T^2 which means the effect of temperature is relatively small compared to that of work function. Because of this, the coefficient of temperature is a modified term and assumed to be 120 $A/cm^2/T^2$. Richard-Dushman's equation does not only reveal the exponential relationship between electron emission and work function, but also indicates that work function is directly proportional to temperature at a given emission density, so it is clear that high temperature yields high work function. Using the concept of work function, Schottky estimated that for a pure metal the energy required to overcome the force of the released electron ϕ_0 is approximately:

$$\phi_0 \approx \frac{7.2}{r}$$

where r is atomic radius of the metal in angstrom. The calculated work function for tungsten using this equation is 4.5 eV, with the atomic radius of tungsten being 1.6 angstrom. This value of work function is the baseline for comparison when the surface of a cathode is coated with additional materials.

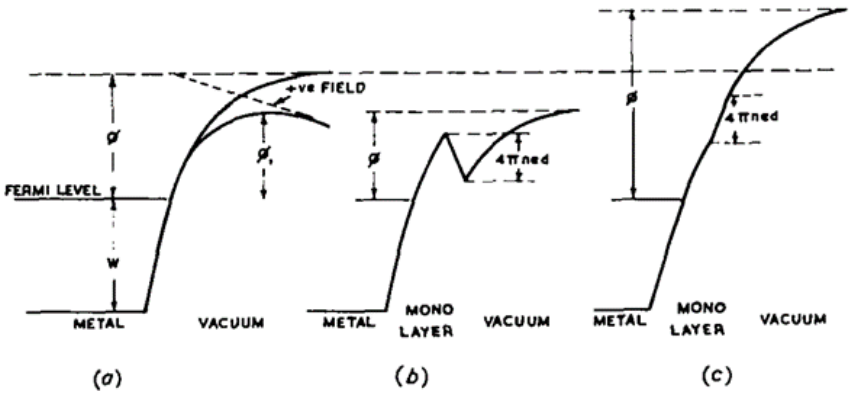

Figure 1.1 [1] Surface function of a) pure metal surfaces coated with b) an electropositive monolayer and c) an electronegative monolayer

High electron emission and low work function are the key characteristics in cathode applications. Electron emission and work function can be either greatly enhanced or deteriorated depending on the electronegativity of the added adsorbate on the surface of a cathode. If the added adsorbate is electropositive with the surface, the atoms in the adsorbate become polarized which will reduce the work function as shown in Figure 1c. The separation distance caused by polarization is denoted as d in Figure 2. The reduction of work function equals to:

$$\Delta\phi = 4\pi \, e \, n \, d$$

where e is the charge due to polarization, and n is the number of atoms absorbed per unit area (cm^2). N is in the order of 10^{14} atoms per cm^2 for a monolayer adsorbate. It is very likely that the electropositive adsorbate is fully ionized and the separation distance becomes the same order of atomic radius of the metal. The change of separation distance contributes to the reduction of work function by 3 eV, and electron emission also increases as a consequence. This is the activation process, shown in Figure 1c, and is favorable. On the contrary, if the adsorbate is electronegative with the cathode surface, the adsorbate becomes negatively charged, attracting the oxidizing gases left in vacuum system, causing

contamination. So an electronegative adsorbate leads to higher value of work function, shown in Figure 1b, and lower value of electron emission. This is not favorable.

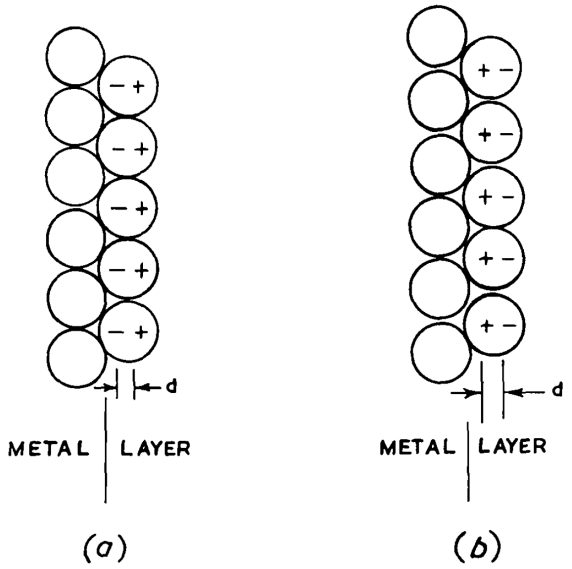

Figure 1.2 [1] Surface of a) an electropositive adsorbate and b) an electronegative adsorbate on a cathode surface.

1.2 Overview on thermionic cathode development

Most conventional thermionic cathodes are made with tungsten because of its high melting temperature and coated with a monolayer of boride or alkaline earth metal oxide on tungsten surface to lower work function and enhance electron emission, because monolayer is stable and yields great electron emission. The monolayer needs to satisfy certain conditions for a cathode to function. First, the coated surface monolayer must have low work function. Second, the binding energy of tungsten and the monolayer must be greater than the binding energy of tungsten and any other deposited materials or contaminations that may be present in the vacuum environment. Third, the monolayer often evaporates at operating temperature, so it must have slow evaporation rate. Last, because the monolayer evaporates, it must be replenished at a certain rate that is neither too fast to cause presence of excessive coating materials, which will lead to small work function

reduction, nor too slow to not supply sufficient coverage. Under these limitations, the monolayer candidates are thorium oxide ThO_2, barium oxide BaO, barium calcium aluminate $(BaO)_3Al_2O_3$, and barium strontium oxide BaO SrO. Table 2 shows the reaction and achievable work function of cathodes with these monolayers at their own operating temperatures. There are also other choices of feasible monolayer that has been developed. For example, thorium oxide on tungsten has a work function around 3.1 eV at 2000 K. It has a unique advantage of not getting permanent damage when working in air. Rare earth metal oxides such as gadolinia and yttria on tungsten have work function of 2.8 eV at 1500 K. They have similar performance of work function and electron emission with thoria-tungsten cathodes, but there are only few applications.

Table 1.2 [1] Achievable Work Function of Cathodes with Commonly-used Monolayers at their Own Operating Temperatures

Cathode	Work function (eV)
Thorium oxide coated on tungsten carbide: $ThO_2 + 2W_2C \rightarrow 4W + 2CO + Th$	2.7 eV at 2200 K
Barium oxide on tungsten: $6BaO + W \rightarrow Ba_3WO_6 + 3Ba$	2 eV at 1200 – 1400 K
Barium calcium aluminate on tungsten: $6(BaO)_3Al_2O_3 + W \rightarrow Ba_3WO_6 + 6(BaO)_2Al_2O_3 + 3Ba$	2 eV at 1200 – 1400 K
Barium strontium oxide mixed with small percent of calcium on pure nickel (indirectly heated cathode)	1.5 eV at 1000 K

Since 1990s, cathodes with a chemical complex consisting of W and Sc_2O_3, impregnated with a 411 mixture of BaO, CaO and Al_2O_3 has been investigated and the discoveries show even more promising improvement in work function for both un-impregnated and impregnated cathodes after activation. Yamamoto *et al* were able to prove that the work function of a W-$Sc_2W_3O_{12}$ coated impregnated cathode was lowered to approximately 1.15 eV at 1342 K after activation. Gibson *et al* found that scandium oxide

and Ba form a Ba-O-Sc chemical complex which results in a work function of 1.5 eV, and that tungsten only serves as an inert support of the complex and does not seem to contribute to the low work function. Zagwijn *et al* established a model system mimicking the behaviors of Sc, Ba, and O on tungsten (001) plane. They confirmed the Gibson *el al* speculation that tungsten is indeed an inert support of the chemical complex and has no role in the enhancement of work function. Besides the experiments done by those who are mentioned above, the emission density of multiple scandia cathode applications is also measured and the result is significantly higher than that of any other types of conventional cathodes. This phenomenon is quite intriguing and has been confirmed experimentally and with model simulations, but the actual working mechanism behind it remains unsolved. Besides the work mechanism of scandia, researchers are also facing many unsolved problems. For example, what role does Ba play when Ba comes to the surface from the dispenser cathode during activation, how does Ba transmit through tungsten-scandia layer, etc.

The application of scandia cathode have disadvantages as well. The biggest problem it is facing right now is the nonuniformity and instability of emission. The nonuniformity, represented by $\frac{\Delta J}{<J>}$ in Figure 3, is 66% at 934 K.

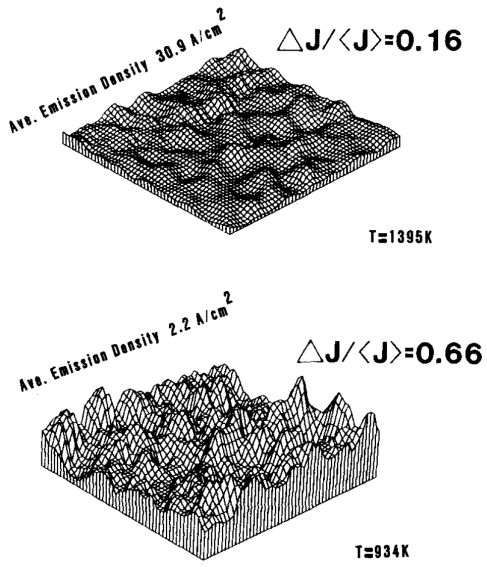

Figure 1.3 [2] Emission density map of a scandia cathode

1.3 Work function of a tungsten-scandia cathode

In Gibson *et al* experiment, the tungsten-scandia cathodes that are impregnated with a chemical complex consisting of BaO, CaO, and Al_2O_3 with a 411 ratio are obtained from a third party. They are tested in a vacuum chamber of 2×10^{-10} torr for both emission density and work function as a function of temperature. Figure 4 is a plot of emission current density versus square root of pulse voltage for the cathode sample at a temperature range from 905 K to 1416 K. This plot demonstrates that above 1100 K the emission density is affected by space charge effect. Figure 5 is a plot of work function calculated from the Richardson-Dushmann equation as a function of operating temperature, ranging from 900 K to 1300 K. It shows a linear relationship between work function and temperature. The slope of the line from 900 K to 1100 K is smaller than that of above 1100 K, so the work function increases more rapidly above 1100 K. Figure 6 is the final results of work function of different materials. By comparison, the monolayer of BaO on W cathode performs the same as the boride cathode. The work function is 2 eV. Scandia

cathode and Ba-activated scandia cathode have the best performance. Their work function is 1.5 eV. Because the interatomic Auger signature of Ba-O bond varies under different chemical environments of Ba and O, this same value of work function of the two types of cathodes suggests that the Ba-activated Sc_2O_3 has the same Auger signature as scandia cathode. For the case of Ba-activated Sc_2O_3, there is no tungsten so Ba-O-Sc chemical complex is created by adding Ba to Sc_2O_3. This confirms that tungsten does not play any role in the enhancement of work function. However, conclusion does not necessarily mean the role of tungsten in forming the chemical complex is denied.

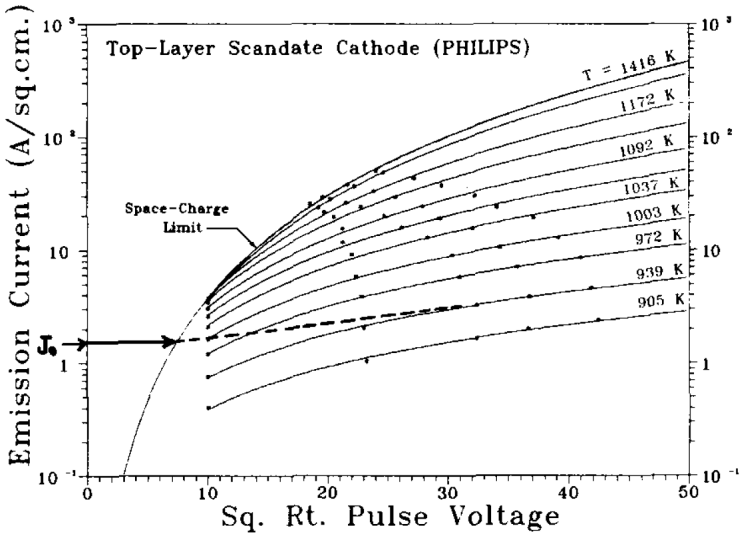

Figure 1.4 [2] Plot of emission current density at different temperatures

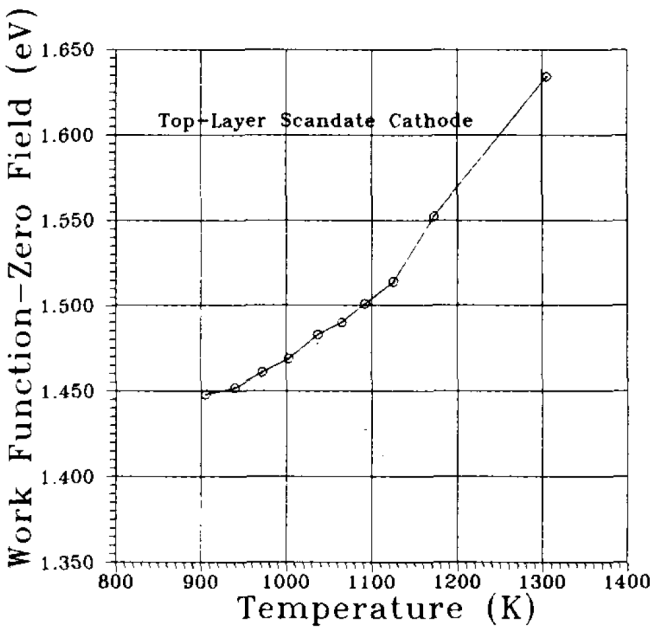

Figure 1.5 [2] Plot of work function calculated by the Richardson-Dushmann equation as a function of operating temperature

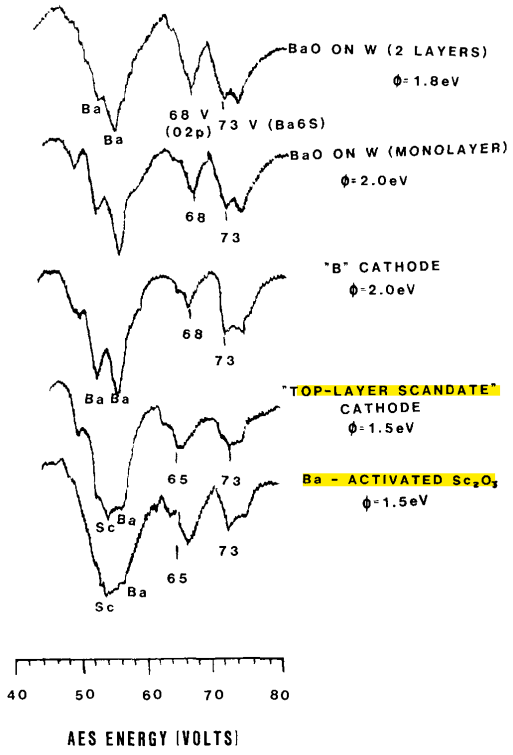

Figure 1.6 [2] Work function of different types of cathode coatings

1.4 Work function of W-$Sc_2W_3O_{12}$ coated cathode

In Yamamoto *et al* experiment, a W-$Sc_2W_3O_{12}$ coated cathode impregnated with Ba is artificially aged at 1423 K within a certain time frame. As shown in Figure 7, the as-prepared cathode has a work function of 4.1 eV. When the activation process first starts at 1423 K, the work function of the cathode is reduced to 2.2 eV. As the activation process progresses at the same temperature, the work function is slowly lowered within the first two hours. After two hours it is slowly increased. The work function is at its minimum of 1.15 eV at 2 hours of artificially aging. After 20 hours the work function is 1.4 eV. The minimum work function of the cathode is lower than any impregnated cathode developed.

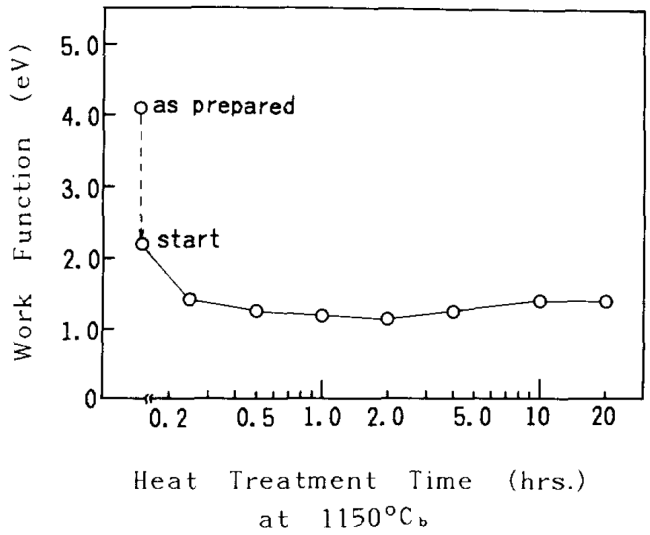

Figure 1.7 [3] Plot of change of work function with respect to time of a W-$Sc_2W_3O_{12}$ coated cathode (impregnated by Ba).

1.5 Work function of Ba-O-Sc on W (001) plane

Zagwijn *et al* establishes a model system of Ba-O-Sc on W (001) plane and compares the model system with a real scandia cathode. In the model system, the sample of tungsten (001) plane is modified, polished, and chemically etched for Auger electron spectroscopy in high vacuum chamber. Surface contaminations except oxygen and carbon

are removed by spattering argon ions. Carbon is removed by raising the temperature to 1500 K in an oxygen rich environment. Oxygen is removed by flashing the surface to 2500 K. These two processes are repeated until the coverage percentage of oxygen and carbon is below 1%. Ba and Sc are deposited in-situ from a oxide-free cathode source, but it is inevitable that minor contamination of oxygen and carbon comes along during the deposition of Sc. The Ba layer is annealed at 1100 K for 1 minute and the deposited sample surface is exposed at room temperature in the high vacuum chamber. For the real scandia cathode, the Auger electron spectroscopy measurement is taken in a completely different set-up from the model system. The results of Auger electron spectroscopy of these two set-ups, as shown in Figure 8, are very similar if the contamination of carbon which is induced during Sc deposition is ignored. The similarities of shape and magnitude of Sc, O, and Ba peaks indicate that the model system mimics the behavior of a real scandia cathode successfully, therefore can be used in work function and emission properties measurements.

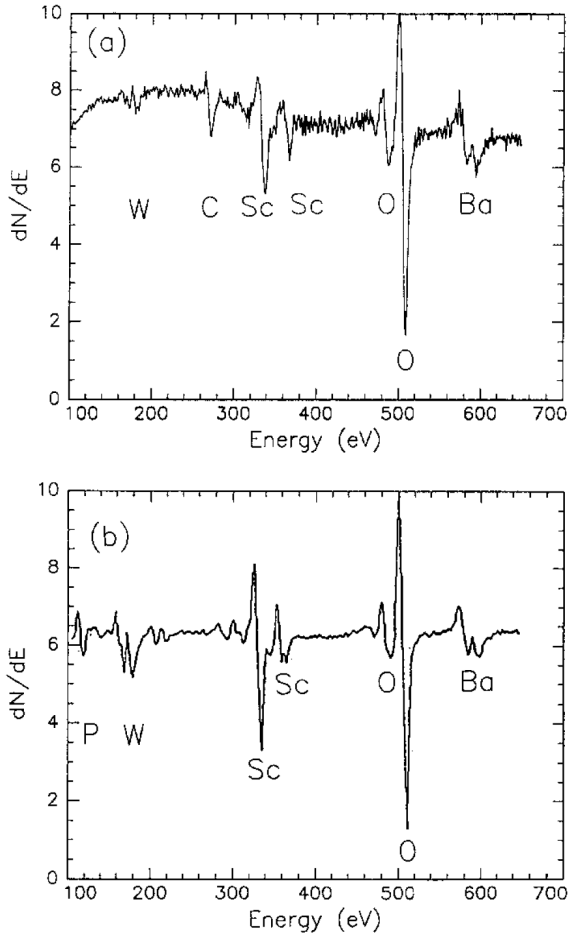

Figure 1.8 [4] Auger electron spectra of a) a modeling system of Ba-O-Sc on W (001) surface, and of b) a real scandia cathode.

The work function of the W (001) plane is measured as a function of Ba coverage as demonstrated in Figure 9. The work function keeps decreasing until the Ba coverage reaches 0.26 ML, and increases slightly until Ba coverage reaches 0.46 ML, then increases dramatically until it plateaus out at approximately 10 ML. The minimum work function shown in this plot is 1.39 eV at 0.28 ML Ba. Noted that the within the range of 0.28 ML Ba coverage, the continuously decreased work function is more linear. This suggests there is a dipole movement due to the difference in electronegative of the surface and adsorbate which has been discussed in Section 1.2. As more Ba is deposited on the tungsten surface,

the Ba-W dipole movement decreases and the work function decreases and plateaus outs to a certain point, and finally increases. Eventually, as the coverage continuously increases and Ba coverage becomes multilayered, the work function is getting closer to that of the bulk Ba coverage value. The work function of W (001) plane as a function of Sc coverage shows similar trend to that of Ba coverage. The minimum work function of 1.83 eV occurs at 1 ML of Sc coverage. After this point the work function increases. As Sc coverage gets close to the bulk coverage, around 10 ML, the work function in increased to 3.33 eV.

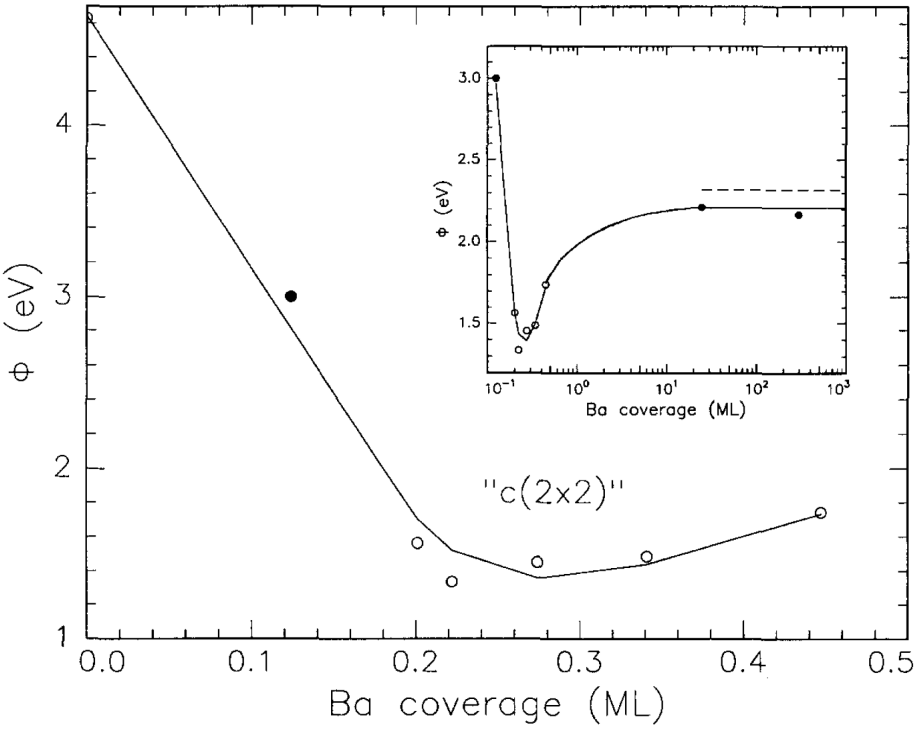

Figure 1.9 [4] Work function of W (001) plane as a function of Ba coverage.

The work function is further decreased when oxygen is absorbed on the Ba-and-Sc-covered W (001) plane. It is decreased to 1.27 eV at the beginning of adsorption as shown in Figure 10. This low value of work function is more superior than that of conventional BaO coated cathode which is 2 eV. The trend of change of work function with respect to O_2 coverage is again, similar to that of Ba and Sc coverage: the work function starts to

increase at 1.5 L of O_2 exposure, stays relatively unchanged from 2 to 3 L of O_2 exposure, and finally increases to a saturation value at around 2 eV above 12 L of O2 exposure. The exposure of O_2 yields identical results (qualitatively) of work function as Ba (0.28 ML) and Sc (1 ML) do. The achievable minimum work function of 1.18 eV in this case fits the optimal work function range for ideal scandia cathode, 1.13 – 1.22 eV.

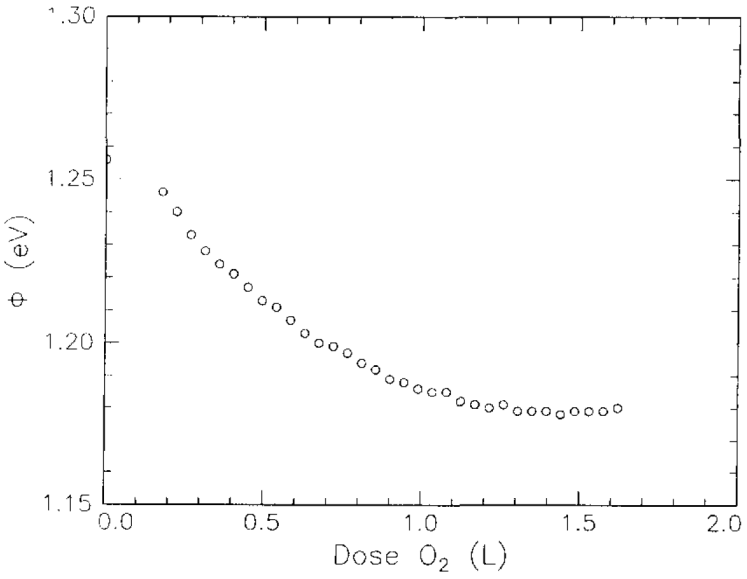

Figure 1.10 [4] Work function with respect to oxygen absorption on W (001) plane coated with Ba and Sc.

CHAPTER 2. EXPERIMENTAL PROCEDURES

2.1 Powder characterization

The scandia nano-powder and the pre-sintered tungsten scandia mix powder were provided by nGimat LLC. The former was made via a nano-spray combustion chemical vapor condensation (nCCVC) system at 99% purity. Transmission electron microscopy (TEM; Joel 2000) was used on the as-made and annealed scandia nano-powder to observe the shape change and size uniformity of scandia crystals.

The pre-sintered tungsten scandia mix powder was examined with scanning electron microscopy (SEM; FEI Quanta FEG 250), energy dispersive spectroscopy (EDS; Oxford X-Max detector with AZtec software), and X-ray photoelectron spectroscopy (XPS). Initially five pre-sintered tungsten scandia loose powder samples which were processed using different mixing conditions were characterized. Of the five samples, one that was determined by comparison of SEM micrographs to have the highest amount of scandia and most uniform coverage was selected. The mixing parameters for this sample were used to make an additional 11 powder sets, denoted with Roman numerals. Differences between these 11 sets were due to intentional and systematic variations in tungsten particles size and the amount of scandia included in each set. On a scale of 1 to 5, with 1 being the least scandia coverage and 5 being the most coverage, each powder set was assigned a number to qualitatively indicate its scandia coverage. Chemical composition and elemental mapping of EDS were performed using the same instrument to provide a quantitative analysis of scandia coverage.

X-ray photoelectron spectrometer (XPS) with copper k alpha wavelength was used on all mix powder sets at high vacuum, $7x10^{-7}$ mbar, to obtain a surface-sensitive

quantification of scandia coverage on tungsten particles. The spot size of the x-ray was adjusted to its maximum, 400 um in diameter, to survey as large area as possible. Four spectra were obtained: tungsten, scandium, oxygen, and carbon. Carbon was included as a reference to correct for peak shift and played no part in quantitative analysis of scandia coverage on tungsten particles. In the C1s spectrum, the peak with its binding energy that was closer to the standard C1s, 286.4 eV, was selected for peak shift correction. Tungsten, scandium, and oxygen peaks were corrected based on how much C1s shifted.

2.2 Cathode pellets characterization

The sintered and impregnated cathode pellets were prepared by Ceradyne, Inc., a 3M Company from its corresponding tungsten scandia mix powder set. The surface morphology and chemical composition for both sintered and impregnated cathode pellets was characterized with SEM and EDS. The cross sections of the sintered and impregnated cathode pellets that was impregnated with $BaO\text{-}CaO\text{-}Al_2O_3$ chemical complex were made and characterized by focus ion beam in a SEM (FEI Helios NanoLab 650) and EDS. The surface work function of sintered and impregnated pellets was measured with a Kelvin probe from KP in ambient environment. The work function of a special designed sintered pellet and its corresponding impregnated pellet, prepared by 3M Ceradyne, was measured in vacuum environment.

CHAPTER 3. RESULTS AND DISCUSSION

3.1 TEM analysis of Sc_2O_3 nano-powder

Figure 3.1 showed the transmission electron microscope (TEM) images of scandia nano-powder in the as-made form and 3 heat treatment forms with different temperature. The shape of scandia particles evolved from round to square and polyhedron during heat treatment, and average particle size became more uniform. The size uniformity of 4 different scandia nano-powder are characterized as shown in Figure 3.2. Reduction in size and improvement in size uniformity as heat treating temperature increases are clearly shown. Change of shape from round (as made condition) to square (HT 1150 ℃ and HT 1300℃) then to polyhedron (1400 ℃). When survey the area, HT 1400 ℃ has the smallest size variation and few particles larger than the average size are found.

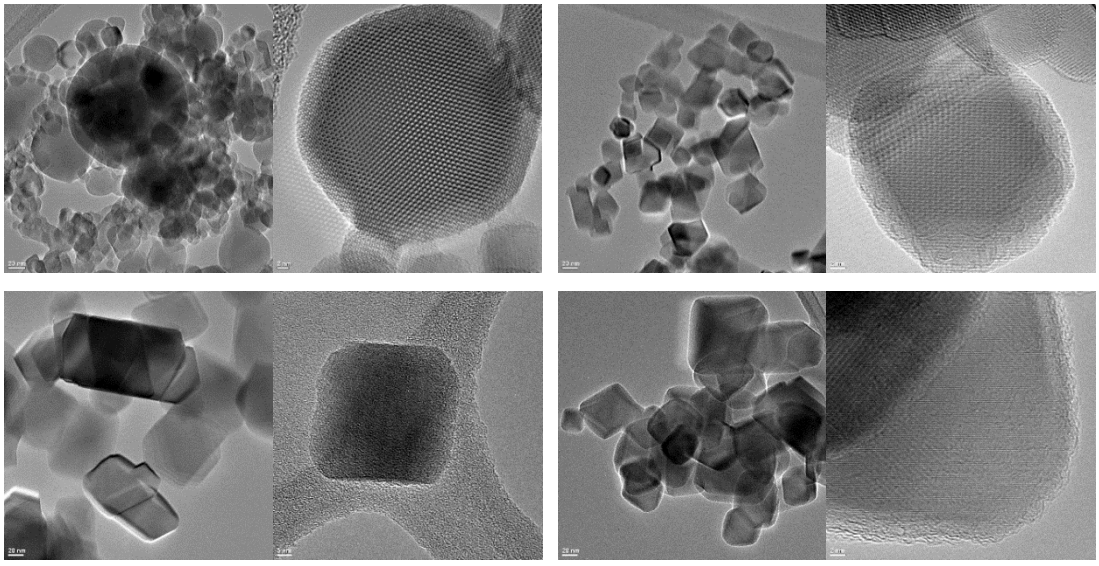

Figure 3.1 TEM images of scandia nano-powder in (a) as-made, heat treated at (b) 1150 ℃, (c) 1300 ℃, and (d) 1400 ℃.

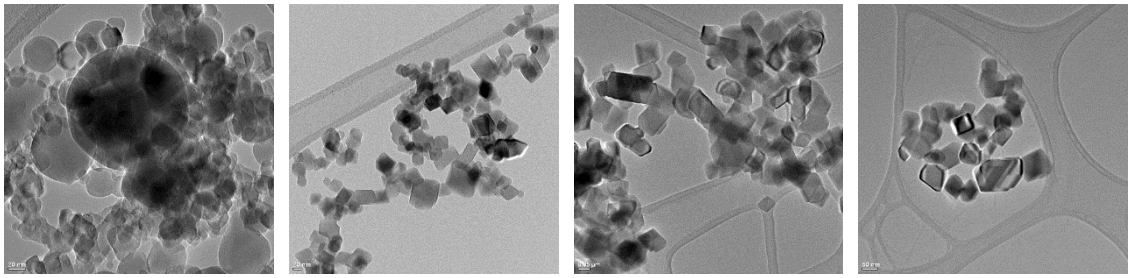

Figure 3.2 A comparison on size uniformity of scandia nano-particle in (a) as made, (b) heat treated at 1150 ℃, (c) heat treated at 1300 ℃, and (d) heat treated at 1400 ℃.

The heat-treated powder particles exhibited more faceting on their surfaces, relative to the as-made powder. High-resolution (lattice) imaging of selected scandia particles reveals the crystallinity of these particles and allows the calculation of interplanar spacing to confirm the lattice parameter of scandia (an example is shown where interplanar spacing was measured as ~3.9 Å, corresponding to {112} lattice planes). Finally, selected-area diffraction patterns and EDS measurements of composition for each powder type corroborate the crystallinity and high purity of these samples, as shown in Figure 3.3 and Figure 3.4 respectively.

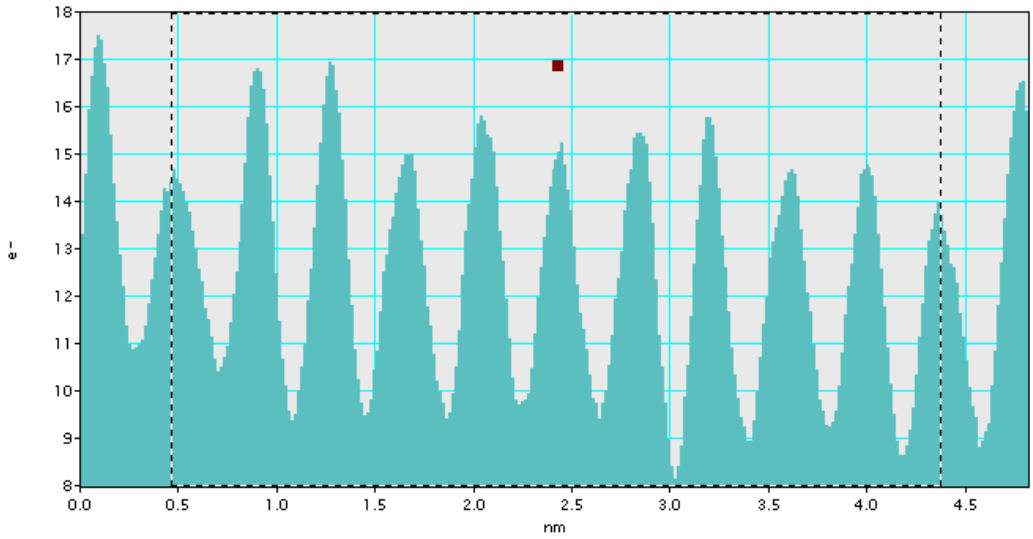

Figure 3.3 Measurement of lattice spacing (~3.9 Å) in heat-treated at 1150 ℃ scandia nano-powder suggests {112} atomic planes.

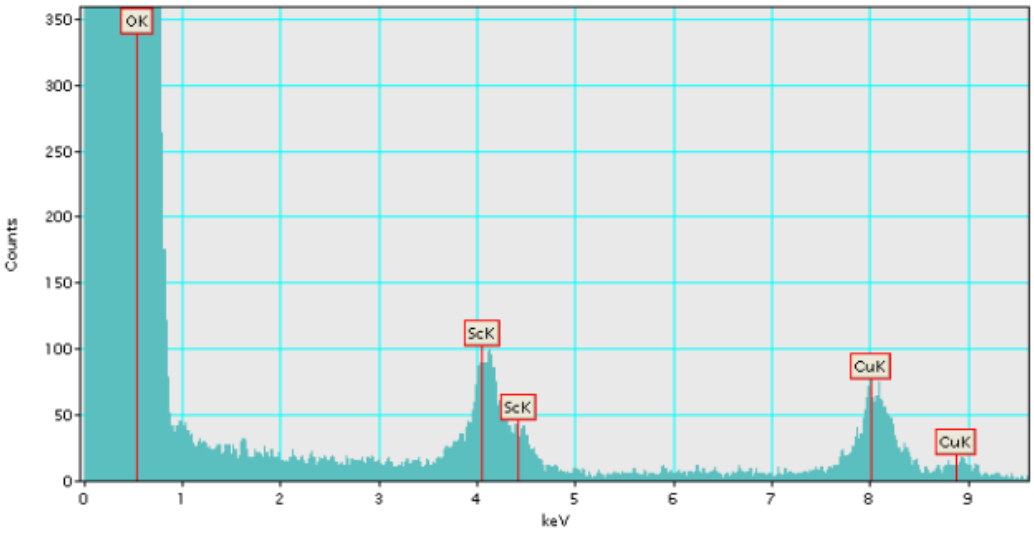

Figure 3.4 EDS measurements elements in the as-made scandia nano-powder. The copper signal is from the supporting sample grid.

3.2 Surface morphology and chemical composition of pre-sintered tungsten scandia mix powder

3.2.1 Surface morphology based on SEM micrographs

On the scale of 1 to 5, with 1 representing the least coverage and 5 representing the most coverage, scandia coverage over tungsten particles of the pre-sintered mix powder set was shown in Table 3.1 and Figure 3.5 and the coverage uniformity was shown in Figure 3.6. Except for scale 1 (Figure 3.6a) that had very poor coverage uniformity, the coverage uniformity of scale 2 to 5 were similar based on visual inspection of SEM micrographs, although coverage uniformity gradually increased and scale 5 had the densest and most uniformity coverage.

Table 3.1 Comparisons between scandia coverage based on qualitative observation of SEM micrographs and quantitative chemical composition analysis from EDS and XPS.

W-Sc2O3 mix powder set #	Coverage scale (1 -5)	Sc at% from EDS	Sc at% from XPS
I	2	6.3	11.16
II	2	6.4	13.36
III	2	6.9	11.91
IV	3	6.7	17.4
V	3	4.6	19.47
VI	**4**	**9.8**	**19.61**
VII	**5**	**11.6**	**21.14**
VIII	**4**	**6.9**	**20.79**
IX	3	6	13.94
X	2	/	12.81
XI	2	2.8	7.5
XIII	1	14.2	9.34

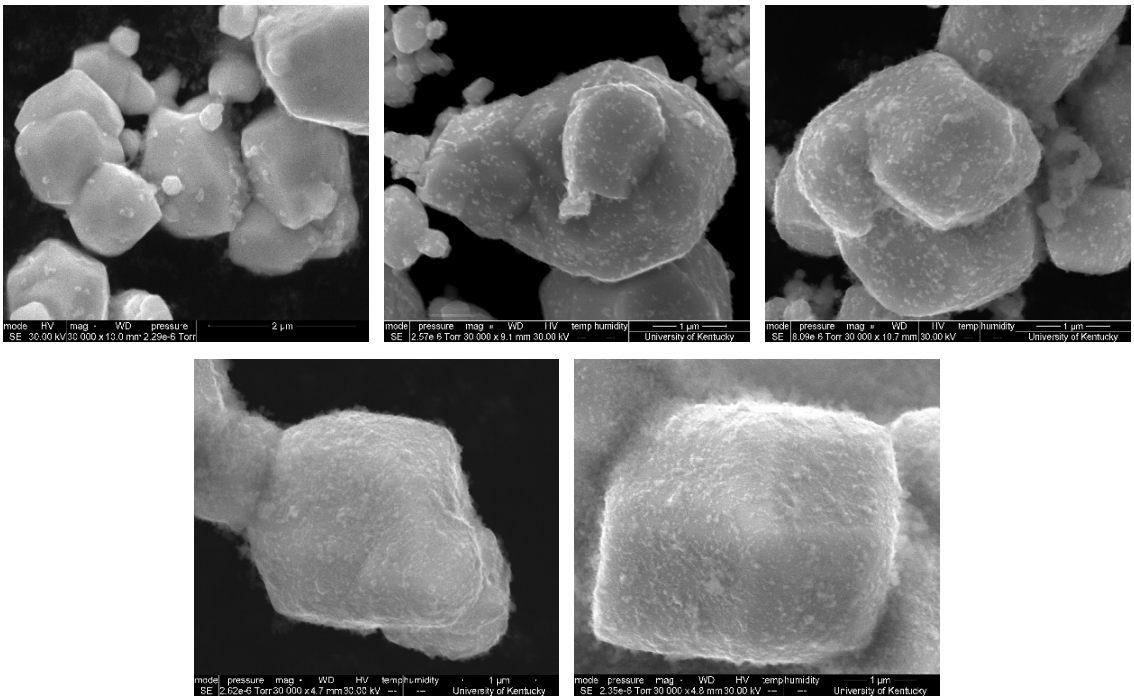

Figure 3.5 SEM micrographs taken in secondary electron imaging mode showing tungsten scandia mix powder. Scandia coverage are defined on a scale of 1 (a) to 5 (e).

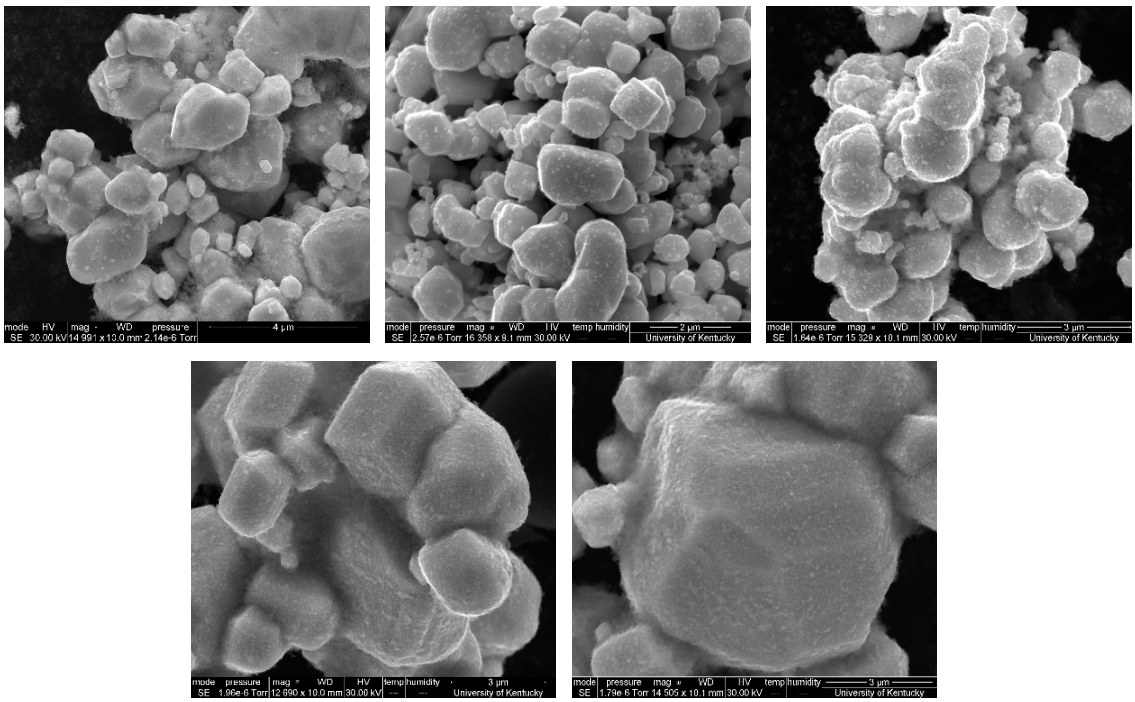

Figure 3.6 Secondary electron SEM micrographs of tungsten scandia mix powder showing coverage uniformity of scale 1 (a) to 5 (e).

3.2.2 Chemical composition analysis based on EDS

Out of the other 12 sets of mix powder, set XIII was found to have the least scandia coverage and many spots with no coverage at all, while set VII was found to have the best uniformity and coverage with no bare spots and few aggregates at tungsten particle boundaries. In set XIII, most scandia aggregated at the boundaries between tungsten particles which was undesired, but it had the highest scandium atomic weight percent, 14.2 at%, among the 12 sets based on elemental mapping analysis of EDS, as shown in Figure 3.7. It was likely that the high atomic weight percent was due to the big lump of scandia mass aggregated between tungsten particles. In set VII, the atomic weight percent of scandium was 11.6% which was the highest of the 12 sets, if set XIII was excluded because the massive aggregation of scandia at tungsten particle boundaries would affect the EDS results. For other mix powder sets, the chemical composition analysis was, in general, consistent with the microstructure observation, as well as the XPS surface analysis which would be discussed in section 3.3. From Table 3.1, it was seen that set VIII had even better coverage and uniformity than that of set VII, but with much less scandium, 6.9 at% and much more oxygen, 45.9%. It was likely that the contribution of oxygen in scandia resulted in the excellent coverage in set VIII because they had abnormally high oxygen at% compared to other sets.

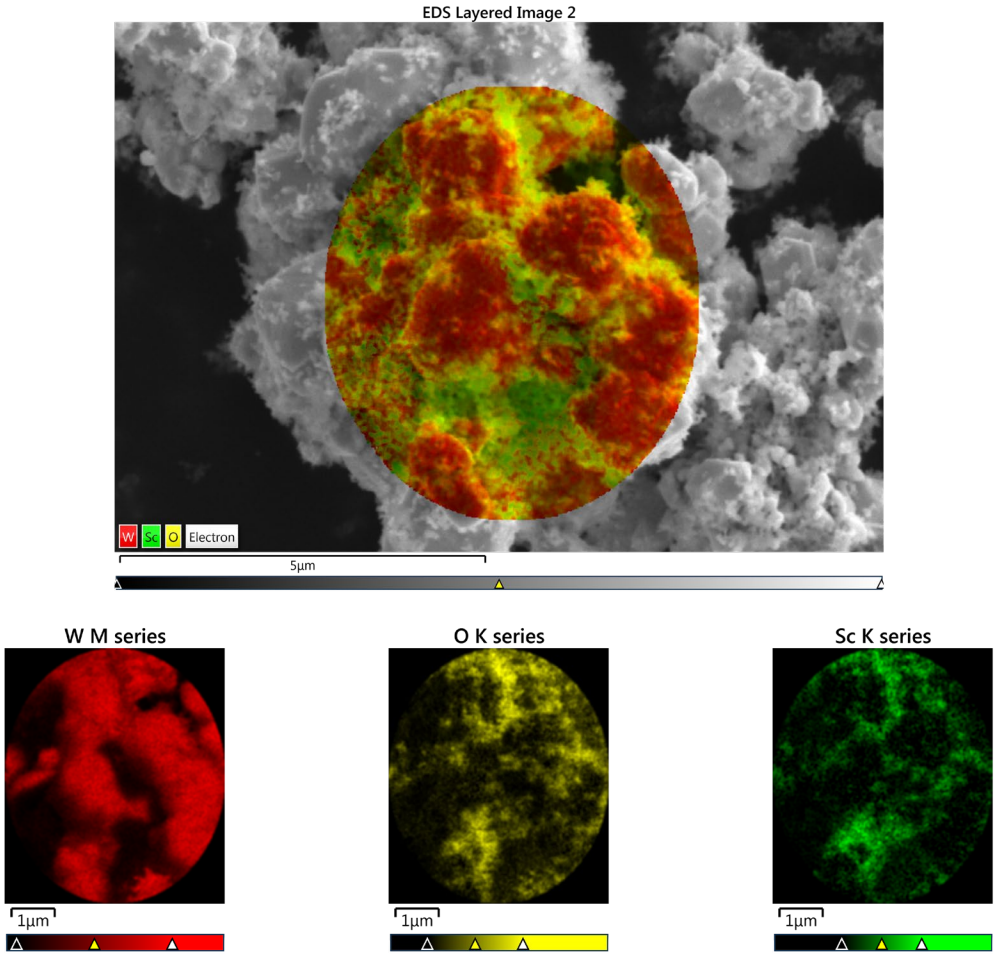

Figure 3.7 EDS layered map (top) and individual elemental map of a level 1 coverage in tungsten scandia mix powder set.

3.2.3 Chemical composition analysis based on XPS

Another quantitative chemical analysis was performed with XPS. The difference between EDS and XPS was that the later had shallower penetration depth and could determine chemical composition as well as binding energy of each element. Due to its surface sensitive nature, the scandia nano-particles would effectively block the tungsten particle underneath, giving the relative areal coverage of scandium on tungsten. After calibration with the reference element, carbon, four spectra for tungsten, scandium,

oxygen, and carbon were corrected for peak shift and shown in Figure 3.8. In the W4f spectrum, there were two pairs of tungsten doublet peaks. The peak doublet on the left of the spectrum was tungsten oxides because it had higher binding energy. vice versa the doublet on the right was metallic tungsten because it had lower binding energy. This held true for all peaks in the spectra. In the O1s spectrum, there should be two peaks because oxygen existed in forms of scandium oxide and tungsten oxide. The oxygen spectrum looked like one peak with its left side slightly widened, which also proved oxygen in the mix powder should have two peaks. After adding the second peak, a well-fitted spectrum was obtained.

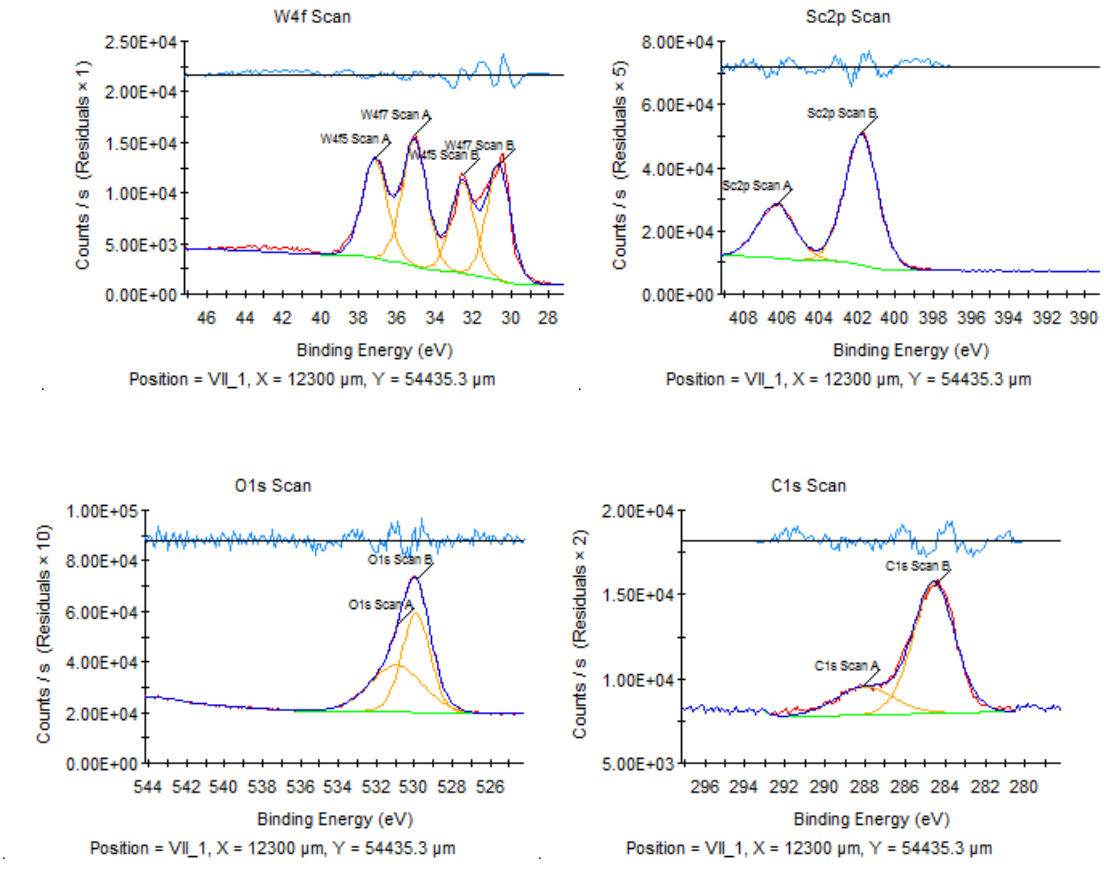

Figure 3.8 XPS measurements for tungsten scandia mix powder set VII.

The XPS quantitative analysis were constructed to compare the relative amount of scandium over tungsten, as shown in Table 3.2. In this analysis, some peaks were excluded, like C1s because it was contamination and only served as a reference to correct for peak shift. It had no part in the quantitative analysis. For any element, the peak with larger area underneath the curve was selected since it had higher signal to noise ratio. Both oxygen peaks were selected because oxygen had as least two forms (scandium oxide, tungsten oxide, and/or other sources) in the mix powder, thus it was trivial to clarify if the peak corresponded to scandium oxide or tungsten oxide. Based on this method, W4f7 scan A, W4f7 scan B, O1s scan A, O1s scan B, and Sc2p scan B peaks were selected in the quantitative analysis. The scandium coverage of set VII was 21.1 at%, the highest among all mix powder sets, and tungsten coverage was 6.82 at%. The ratio of total scandium to total tungsten is approximately 3:1. This ratio was calculated by using all peaks mentioned above except C1s and O1s. The oxygen content was not considered because it might have many sources including contamination. The ratio of other 12 mix powder sets were shown in Table 3.3. The lowest ratio came from set XI and the highest ratio came from set VIII.

Table 3.2 Scandia surface coverage based on quantitative XPS analysis on mix powder set VII.

Name	Peak BE	FWHM eV	Area (P) CPS.eV	Atomic %	Q
W4f7 Scan A	35.06	1.55	20853.87	3.65	1
W4f7 Scan B	30.64	1.47	18157.65	3.17	1
Sc2p Scan B	401.79	2.04	91684.45	21.1	1
O1s Scan A	530.91	3.28	65083.68	33.68	1
O1s Scan B	529.89	1.75	74259.15	38.4	1
W4f5 Scan A	37.16	1.55	16439.54	0	0
W4f5 Scan B	32.54	1.47	14314.06	0	0
C1s Scan A	288.04	3.37	6098.87	0	0
C1s Scan B	284.55	2.45	20458.69	0	0
Sc2p Scan A	406.26	2.26	41648.94	0	0

Table 3.3 XPS analysis summary and total Sc:W ratio representing Sc coverage for all mix powder sets.

Mixed powder set	Atomic % Sc	Atomic % W	Sc:W ratio	Qualitative Assessment
I	11.16	10.45	1.07	2
II	13.36	8.95	1.49	2
III	11.91	17.29	0.69	2
IV	17.4	10.46	1.66	3
V	19.47	9.00	2.16	3
VI	**19.61**	8.46	**2.32**	**4**
VII	**21.14**	6.82	**3.10**	**5**
VIII	**20.79**	5.41	**3.84**	**4**
IX	13.94	9.59	1.45	3
X	12.81	6.80	1.88	2
XI	7.50	16.94	0.44	2
XIII	9.34	9.62	0.97	1

3.2.4 Determination of the highest scandia coverage mix powder set

When trying to determine which mix powder set had the highest coverage, the three different assessment methods of scandia coverage were combined and compared, as shown in Figure 3.9. It demonstrated inconsistent trends between the qualitative and quantitative assessments due to the inaccurate nature of visual observation, however it was likely that the visual observation of scandia coverage could agree with the quantitative analysis if more areas were surveyed and more accurate coverage scale was used, for example 1.5, 2.5, 3.5, etc., because there were mix powder sets that had more coverage compared to others and they were assigned with the same number in the coverage scale. It was determined that set VII had the highest scandia content, although the scandia content in EDS analysis was the second highest to set XIII, which had proven to have little to no scandia coverage on tungsten particles surface but many large aggregates at tungsten particle boundaries. The coverage scale assigned in the qualitative assessment from SEM micrographs and scandium at% obtained in XPS agreed with this decision.

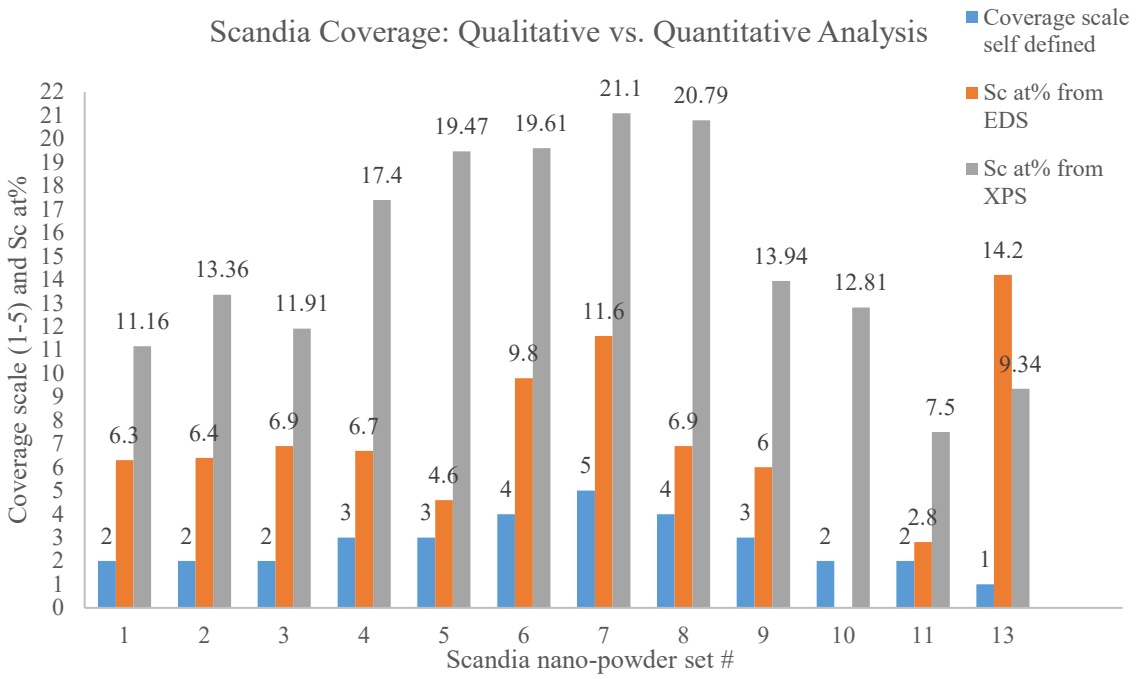

Figure 3.9 Scandia coverage based on qualitative microstructure analysis vs. quantitative EDS and XPS analysis.

3.3 Surface morphology of sintered and impregnated cathode pellets

3.3.1 Sintered cathode pellets

The microstructure of all sintered pellets, as shown in Figure 3.10, was consistent. The primary difference was the number of scandia particles that remained distributed over the tungsten grains. The amount of scandia observed on W after sintering corresponded to the coverage of scandia particles in the mixed powder sets. More scandia coverage resulted in higher amount of scandia distributed over the sintered tungsten.

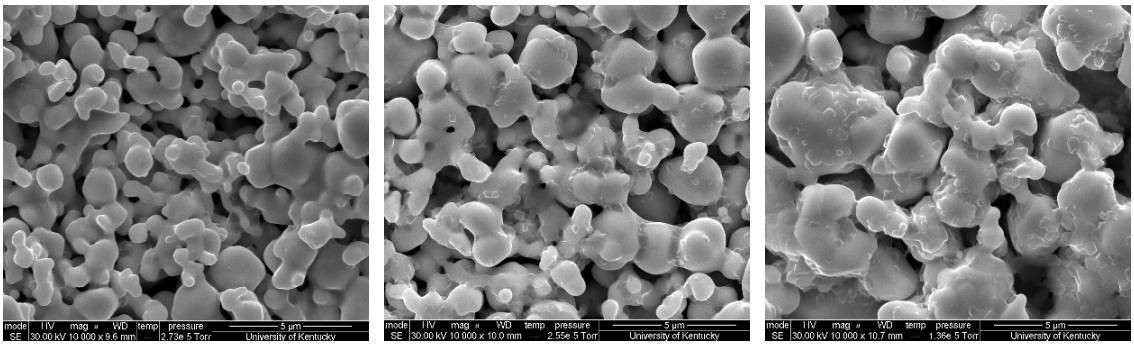

Figure 3.10 Secondary electron SEM micrographs of sintered cathode pellet surface. various sample types are shown including (a) low amount, (b) medium among, and (b) high amount of scandia particles.

An exception that had distinctively different microstructure than any other pellets and whose corresponding mix powder was not manufactured by nGimat LLC was designed with 3-b. The microstructure of two similar pellets and 3-b are shown in Figure 3.11. The pellet showed highly faceted tungsten particles.

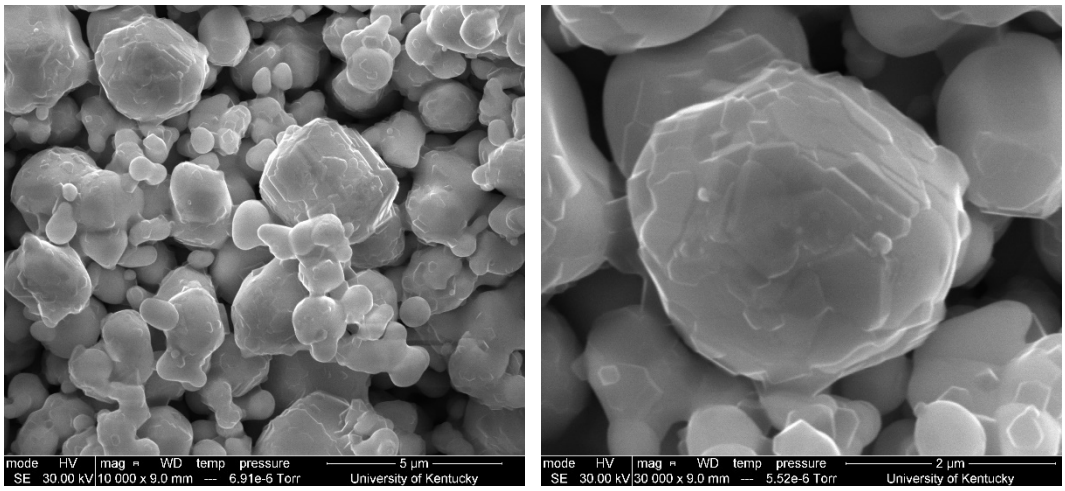

Figure 3.11 Surface morphology of special designated sintered cathode pellet 3-b.

3.3.2 Impregnated cathode pellets

Figure 3.12 showed an SE image (left) and concentric backscattered electron (BSE) image (right) of impregnated pellet VII-B, whose corresponding loose powder was

determined to have highly uniform scandia coverage. Because the impregnated pellet surfaces were heavily machined, the surfaces experienced significant deformation and no meaningful microstructure was observed at the surface.

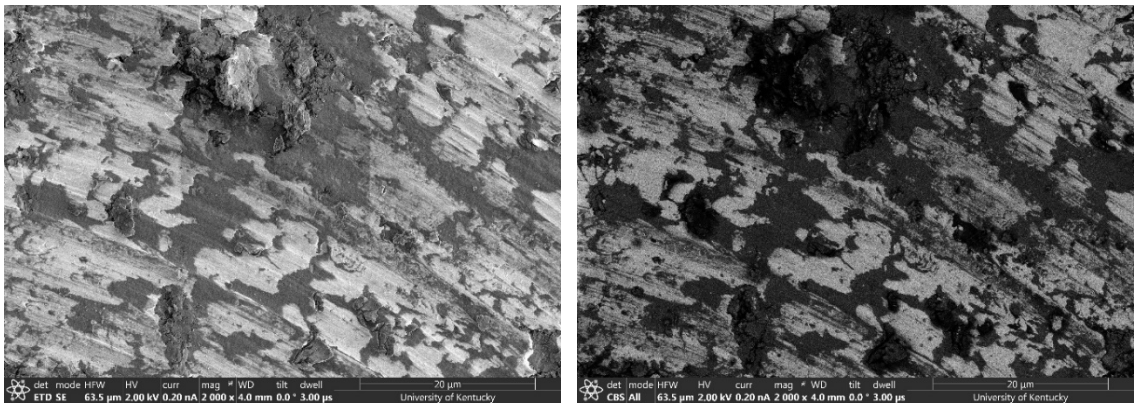

Figure 3.12 SE (left) and BSE (right) images taken at the surface of an impregnated cathode pellet.

However, “holes”, most likely caused by machining, were found on the surface of an impregnated pellet. EDS elemental maps confirmed that beneath the “hole”, the expected elements and compounds from the impregnation step were present, as shown in Figure 3.13. It was noted that calcium was not detected in the same regions as Ba, Al and Sc in the EDS elemental maps, and Ca did not appear to be present in significant amounts after the impregnation step.

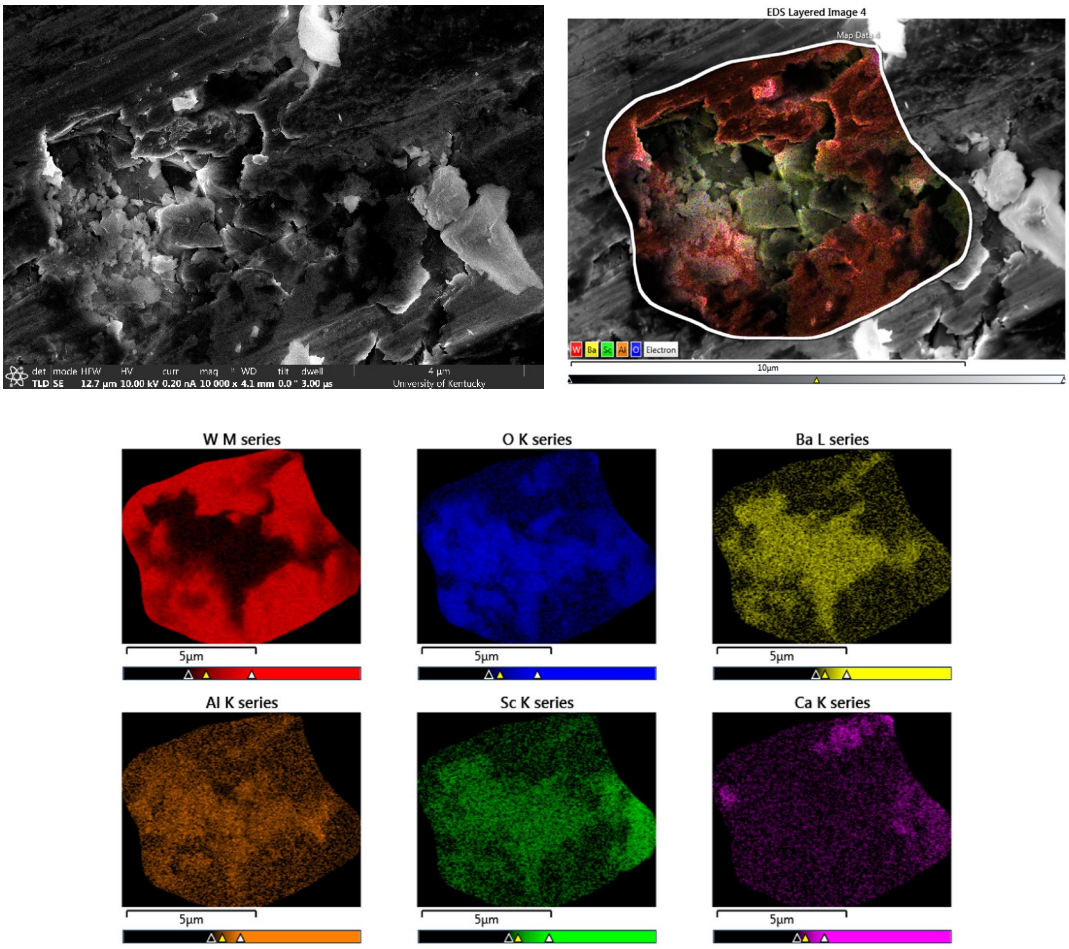

Figure 3.13 EDS elemental mapping of a “hole” on the surface of an impregnated pellet.

3.4 Cross-sectional area analysis of sintered and impregnated cathode pellets

Figure 3.14 showed a cross section made by focus ion beam on sintered pellet surface and its EDS chemical analysis. It was observed in the EDS layered image that tungsten and scandia did not overlap, and the structure of the cross section was porous which was expected in a sintered pellet.

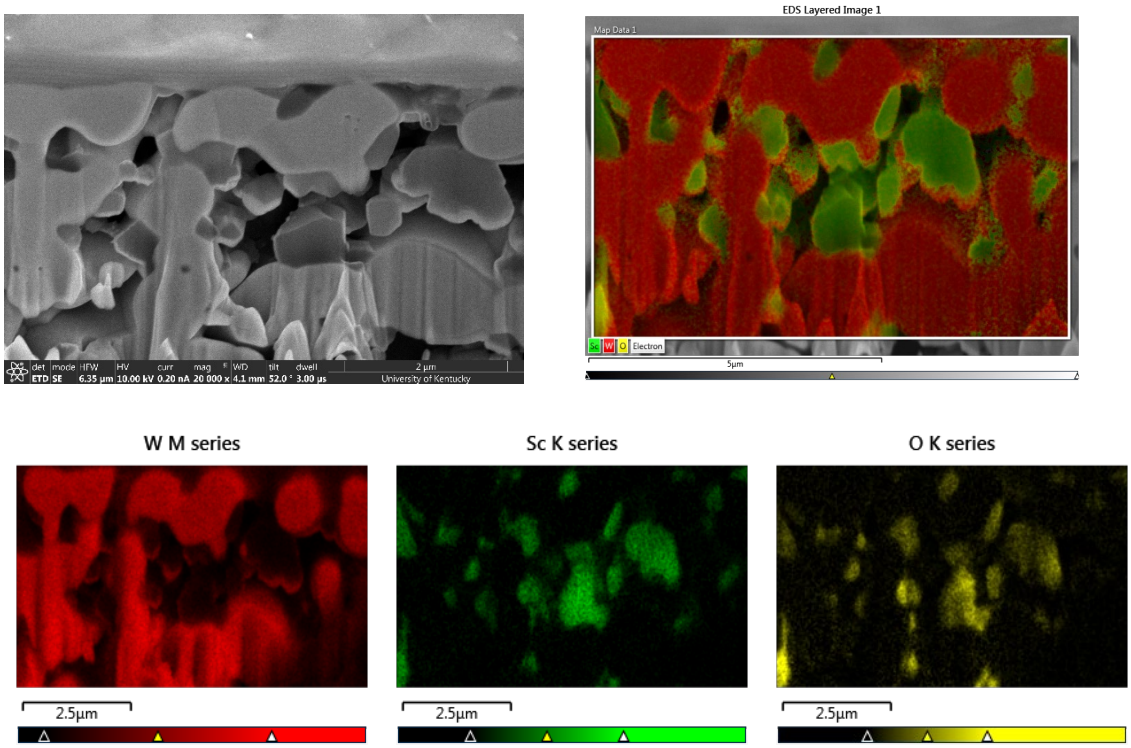

Figure 3.14 Characterization of a cross-sectional area created by FIB SEM and EDS analysis of sintered cathode pellet IV.

Figure 3.15 showed a cross section made by FIB on impregnated pellet surface and its EDS chemical analysis. The impregnated chemical complex which contains various ratio of BaO-CaO-Al2O3 was well mixed, as their elemental maps overlapped together, Al overlapped with Ba and Ca overlapped with Sc. During impregnation, the impregnated chemical complex emerged to the surface and filled the pores therefore it was observed that there were little to no pores left after the impregnation.

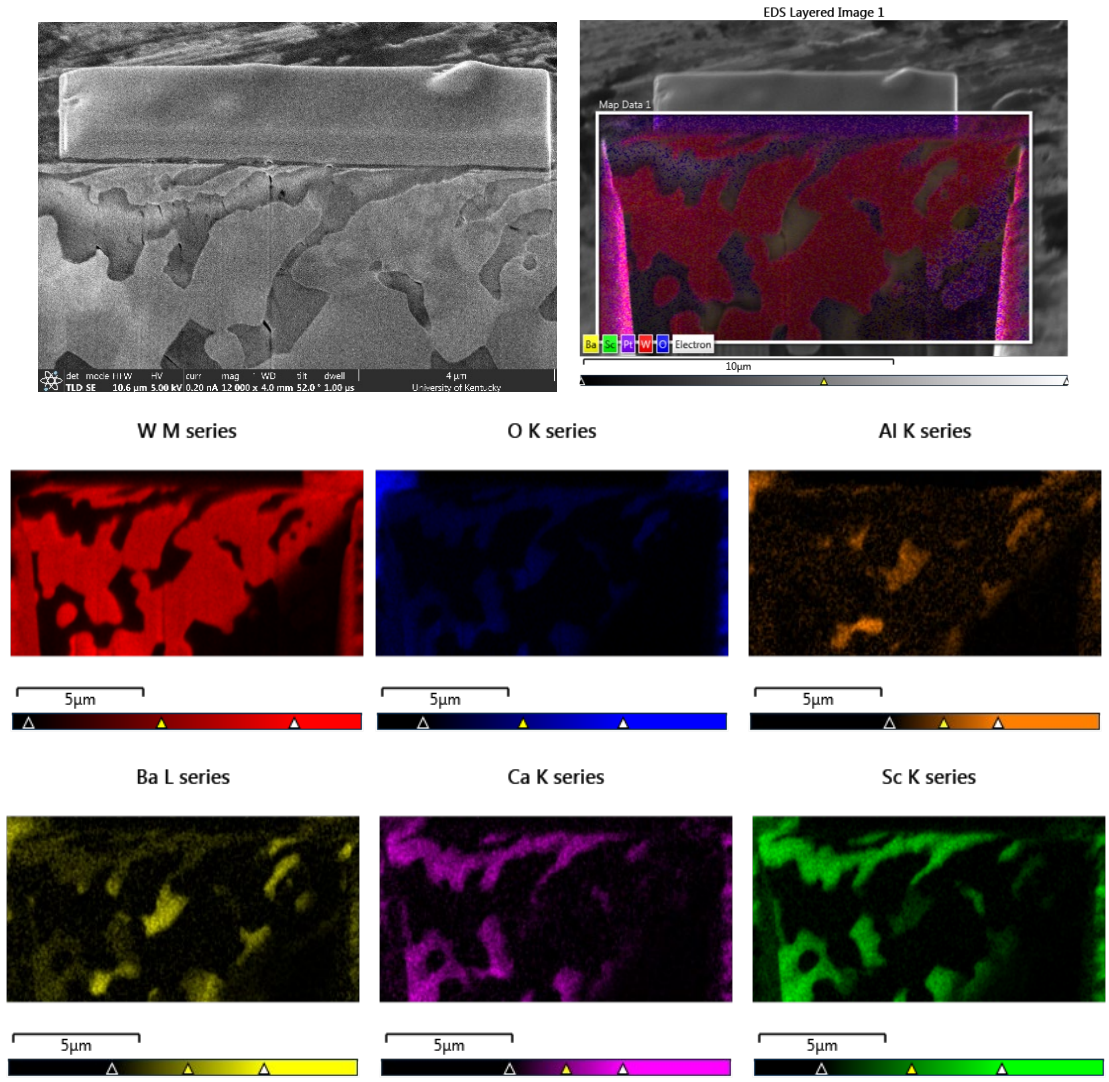

Figure 3.15 Characterization of a cross-sectional area created by FIB SEM and EDS analysis of impregnated cathode pellet IV.

3.5 Work function measured in ambient and vacuum environment of sintered and impregnated cathode pellets

The work function values of several pellet surfaces were measured using a Kelvin probe in ambient environment. The relative work function measured in contact potential difference mode (V_{cpd}) was listed for each measurement in the table below. Relative and absolute values of work function were related by the equation: $\varphi_{sample} = \varphi_{tip} + V_{CPD}$

where φ_{tip} was the work function of the probe tip. Depending on which tip was used φ_{tip} was different, and therefore φ_{tip} could be treated as a reference value. As shown in the Table 3.4, there was little variation in work function within each of the sintered or impregnated pellet sets, but the average difference between sintered and impregnated pellets was significant (on the order of 500 meV, or 0.5 eV). Note that not all sintered and impregnated pellet pair was included since some impregnated pellets were extremely brittle and broken or chipped during the characterization process. Their uneven surface was no longer fit for work function measurement because work function must be measured on a flat surface. However, comparing other available pairs of the sintered vs. impregnated pellets, a clear trend was observed, namely that the surface work function decreased by approximately 0.5 eV after impregnation.

Table 3.4 Comparison of ambient work function between sintered and impregnated cathode pellets.

W-Sc_2O_3 mix powder set	Ambient work function of sintered pellet (eV)	Ambient work function of impregnated pellet (eV)
I	5.09	4.52
II	5.16	4.55
IV	5.25	4.60
VI	5.07	4.47
IX	5.08	4.46

Work function measurements were also performed on pellets 3-b (sintered, but not impregnated) and 3-c (after impregnation) in a vacuum environment. The table below lists work function (eV) for these two pellets, measured first at room temperature (before heating), then at 700˚C, and finally at room temperature after cooling down. These values were calculated with a value of φ_{tip} = 4.350 eV. Calibration of the tip was attempted with a (100)-oriented silicon wafer, which has a work function of 4.8-4.9 eV as quoted from literature. The work function measured at the University of Kentucky for this Si wafer was

4.768 eV, which differs the standard value by less than 0.1 eV. Therefore, it is reasonable to assume a similar error (0.1 eV) for other work function measurements at this point. As shown in the table below, the work function of pellet 3-c decreased significantly due to heating to 700˚ C and remained essentially constant after cooling back down to room temperature. This suggests that the surface measured at 700˚C was largely preserved during cooldown and was not coated with contaminants that would change the work function. The initially higher value of WF for pellet 3-c (before heating) could be due to adsorbed species or contaminants from ambient conditions, which were subsequently driven off by heating. Note that similar analysis for pellet 3-b was not possible, because the WF was not measured before heating.

Table 3.5 A comparison on work function measured in vacuum of special designed 3-b and 3-c

Sample	Room temperature (before heating)		Heated at 700˚C		Room temperature (after heating)	
	Average WF	WF standard deviation	Average WF	WF standard deviation	Average WF	WF standard deviation
3-b (sintered)	/	/	4.26 eV	0.03 eV	4.20 eV	0.01 eV
3-c (impregnated)	4.17 eV	0.02 eV	3.61 eV	0.04 eV	3.63 eV	0.02 eV

CHAPTER 4. CONCLUSIONS AND FUTURE WORK

4.1 Conclusions

Scandate cathode under various processing stages: scandia nano-powder, tungsten scandia mix powder, sintered and impregnated pellets, were characterized with techniques that included electron microscopy, EDS, XPS, and work function measurements.

At the scandia nano-powder stage of processing, the size and shape uniformity of nano-scale scandia particles heat treated at different temperatures were characterized with TEM. The shape changed of scandia nano-particles changed from round to square and polyhedron during heat treatment. Reduction in size and improvement in size uniformity as heat treating temperature increased were observed. The average particle size of a heat-treated sample was around 80 nm.

At the next stage of processing, all tungsten scandia mix powder sets were characterized with SEM, EDS and XPS to determine the highest scandia coverage on tungsten particles. Based on the qualitative assessment with SEM micrograph observations, a customized coverage scale from 1 to 5, with 1 being the least coverage and 5 being the most coverage, was created. Set VI, a scale 4 coverage, VII, a scale 5 coverage, and VIII, a scale 4 coverage, were considered as good coverage featuring a large population and a uniform distribution of scandia. Set XIII, a scale 1 coverage, were considered as poor coverage because their micrographs showed many bare spots with no scandia population and massive scandia aggregation at tungsten particle boundaries. The quantitative assessment with EDS showed an inconsistent trend with the qualitative assessment. It demonstrated that set XIII had the largest scandia at% and XI had the smallest Sc at%. One possible reason for set XIII to have high Sc at% in the EDS was the large amount of scandia

detected at tungsten particle boundaries. Proven to be a poor coverage set in the qualitative assessment, although with high Sc at% in EDS analysis, it should be excluded in the determination of the highest Sc coverage. In this case, set VII had the highest Sc at%. Another quantitative assessment on scandia coverage came from XPS. The results showed that the top three highest Sc at% mix powder sets were VII, 21.14 at% Sc, VIII, 20.79 at% Sc, and VI, 19.61 at% Sc. The mix powder sets that had the top three highest total Sc to W ratio were VIII (Sc:W = 3.84), VII, (Sc:W = 3.10), and VI (Sc:W = 2.32). Combining all three assessment methods, it was concluded that set VII had the highest Sc at%. Its competitor, set VIII, was not selected because it had much lower Sc at% and abnormally higher O at% in EDS analysis. It was likely that the abnormally large amount of oxygen, instead of scandium, was observed in the SEM micrographs.

At the sintered pellet stage, it was observed with SEM that more initial scandia coverage in the mix powder sets corresponded to a larger number of scandia particles distributed over the tungsten surface in a sintered pellet. The structure of the cross section made on pellet surface was porous which was expected in any functional cathode. Kelvin probe measurements revealed that work function values of sintered pellets were similar and, in all case including the special designated pair 3-b and 3-c, decreased by approximately 0.6 eV after the impregnation.

At the impregnation stage of processing, the surface morphology of the pellet was meaningless due to the surface was heavily machined. However, there were “holes” on the surface, and under the surface the expected elements and compounds from the impregnation step were present. A cross section on the pellet surface was made and characterized with SEM and EDS. Figure 3.15 revealed that the pores that existed in

sintered pellets were gone and filled with impregnated materials that emerged to the surface during impregnation.

4.2 Recommendations for future work

More research needs to be done on cathode pellets after activation. Due to the limitation of instrumentation, work function measurements of scandate cathodes after activation in ultra-high vacuum were not feasible, but they will be critical for establishing a correlation between scandia coverage and emission properties, thus prove the effects of scandia distribution on surface structures of scandate cathode. Electron microscopy characterizations of cross sections will also be valuable for comparison of structural changes in pre-activation and activated scandate cathodes.

REFERENCES

[1] A. Van Oostrom, L. Augustus, *Applied Surface Science*, 1979, Vol. 2, p. 1752

[2] J. Hasker, J. J. H. Stofflen, *Applied Surface Science*, 1985, Vol 24, p. 330

[3] J. Hasker, Van Esdonk, J. E. Combeen, Properties and manufacture of top-layer scandate cathodes. *Applied of Surface Science*, 1986, Vol. 26, p. 173

[4] A. Szczepkowicz, *Surface Science*, 2011, Vol. 605, p. 1719-1725

[5] J. W. Gibson, G. A. Haas, R. E. Thomas, *IEEE Transactions of Electron Devices*, 1989, Vol. 36, p. 209

[6] R. Jenkins, *Vacuum*, 1969, Vol. 19(8), p. 353-359

[7] A. Szczepkowicz, R. Bryl, *Surface Science*, 2004, Vol. 559, p. 169-172

[8] C. Herring, *Physics Review*, 1951, Vol. 81, p. 87

[9] S. Yamamoto, I. Watanabe, S. Sasaki, T. Yaguchi, *Vacuum*, 1990, Vol. 41 (7-9), p. 1762

[10] P. M. Zagwijn, J. W. M. Freken, U. van Slooten, P. A. Duine, A model system for scandate cathodes, *Applied Surface Science*, 1997, Vol. 35, p. 41

[11] A. Szczepkowicz, A. Ciszewski, R. Bryl, C. Oleksy, C. H. Nien, Q. Wu, T. E. Madey, *Surface Science*, 2005, Vol. 599, p. 55-68

[12] S. Fujita, H. Shimoyama, *Journal of Vacuum Science & Technology*, 2008, Vol. B 26 (2), p. 738-744

[13] D. Niewieczerzal, C. Oleksy, *Surface Science*, 2006, Vol. 600, p. 56-65

[14] W. Shuguang, *Applied Surface Science*, 2005, Vol. 251, p. 114-119

[15] S. Yamanoto, I. Watanabe, S. Sasaki, T. Yaguchi, *Surface Science*, 1992, Vol. 266, p. 100

[16] G. Gartner, P. Geittner, H. Lydtin, A. Ritz, *Applied Surface Science*, 1997, Vol. 111, p. 11 – 17

[17] Y. Wang, Z. X. Song, D. Ma, X. Y. Wei, K. Xu, *Surface & Coatings Technology*, 2007, Vol. 201, p. 5518 – 5521

[18] G. Wulff in *Z. Kristallogr. Miner*, 34 (1901) 993

[19] N. Akutsu, Y. Akutsu, *Journal of the Physical Society of Japan*, 1987, Vol. 56 (7), p. 2248 – 2251

[20] C. Rottman, M. Wortis, *Physics Review*, 1984, Vol. B29, p. 328

[21] Zhang, X., Balk, J., Hunt, A., and Busbaher, D., Effects of scandia distribution on surface structure of scandate cathodes. *International Vacuum Electronic Conference*, 2018

[22] Wang, Y., J. Wang, W. Liu, K. Zhang, and J. Li, Development of High Current-Density Cathodes with Scandia-doped Tungsten Powders, *IEEE Transactions on Electron Devices*, vol. 54, no. 5, pp. 1061-1071, 2007

[23] Thomas, R. E., J. W. Gibson, G. A. Haas, and R. H. Abrams, Thermionic Sources for High-Brightness Electron Beams, *IEEE Transactions on Electron Devices*, vol. 37, no. 3, pp. 850-861, 1990

[24] Liu, X., Zhou, Q., Maxwell, T. L., Vancil, B., Beck, M. J., and Balk, J., characterization of a scandate cathode: high-resolution imaging, chemical analysis, and emission testing, submitted to *Applied Surface Science*.

[25] Zhou, Q., Liu, X., Maxwell, T. L., Vancil, B., Balk, J., and Beck, M. J., Investigation of surface properties for scandate cathodes: DFT study of adsorption on W (001), (110), (112) and crystal shape," submitted to *Applied Surface Science*.

VITA

Xiaomeng Zhang received her B.S. degree in Materials Science and Engineering in May 2016 from Purdue University. She continued her study as a master student and joined Dr. John Balk's group at the University of Kentucky in August 2017.